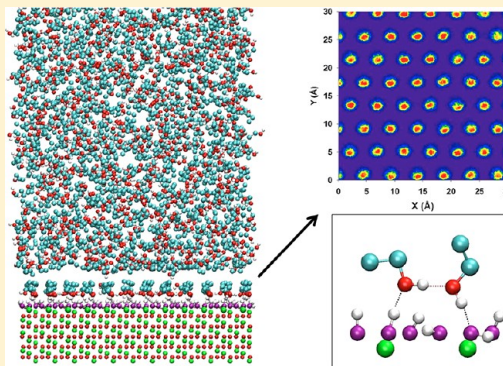


Liquid Ethanol Simulated on Crystalline Alpha Alumina

Anh Phan,[†] David R. Cole,[‡] and Alberto Striolo^{*,†}[†]School of Chemical, Biological, and Materials Engineering, University of Oklahoma, Norman, Oklahoma 73019, United States[‡]School of Earth Sciences, The Ohio State University, Columbus, Ohio 43210, United States

S Supporting Information

ABSTRACT: Equilibrium molecular dynamics simulations were employed to investigate the structural properties of interfacial liquid ethanol on two alumina surfaces—the (0001) and the (1 $\bar{1}$ 02) terminations of α -Al₂O₃—both described using the CLAYFF force field. The resultant atomic density profiles show that ethanol molecules in the first monolayer are well ordered and that their distribution depends on the surface OH groups. A pronounced dipolar orientation is found for the ethanol molecules in the first layer and also, although to a smaller extent, among the ethanol molecules in the second molecular layer. The orientational distribution predicted for the methyl group of ethanol on α -Al₂O₃ (1 $\bar{1}$ 02) is consistent with that observed experimentally by Shen and co-workers. The orientation of molecules in the second layer is opposite compared to that found in the first adsorbed molecular layer. Our simulations show long residence times and slowly decaying reorientation autocorrelation functions for ethanol molecules in the first adsorbed layer, suggesting that within the first adsorbed layer ethanol molecules are strongly coordinated with both α -Al₂O₃ (0001) and α -Al₂O₃ (1 $\bar{1}$ 02) surfaces. Analysis of the hydrogen bond network confirms that preferential surface–ethanol interactions are responsible for such observations.



■ INTRODUCTION

Understanding the microscopic properties of hydrogen-bonding (HB) liquids at solid–liquid interfaces is important for many chemical and biological processes.^{1–5} While liquid water has been the popular subject of numerous experimental^{6–9} and computational studies,^{10–19} only a few investigations have been carried out for other HB liquids, including alcohols. These are expected to yield tridimensional HB patterns different compared to those typical of liquid water at interfaces.²⁰ Several industrial, geophysical, petroleum, and environmental applications employ amphiphilic molecules in contact with solid substrates.

Among other alcohols, an increasing number of computer simulation studies focused on bulk liquid ethanol are being reported in the literature.^{20–26} For example, Saiz et al.²⁰ employed molecular dynamics (MD) simulations to study structure and dynamics of liquid ethanol at four thermodynamic states using the transferable optimized potential model for liquid simulations (OPLS) force field.²⁷ The results were in overall agreement with available experiments for, e.g., bulk density and diffusion coefficients.^{28–30} The OPLS force field was also used by Wensink and co-workers to study dynamical properties of water/alcohol mixtures.²³ More computational demanding polarizable and flexible models have also been developed. Wang and Cann,²⁵ e.g., used ab initio B3LYP/6-311++G(d,p) data to parametrize accurate force fields for ethanol. Although polarizable and flexible models appear to be essential for modeling complex biological systems,^{25,31–34} Noskov et al.²⁴ showed that results for enthalpy of evaporation,

molecular volume, dielectric constant, and self-diffusion coefficient obtained by implementing polarizable force fields are comparable to those obtained by using nonpolarizable force fields. Noskov et al.²⁴ noted that polarizable force fields should be used to accurately predict the dielectric constant and minima in the self-diffusion coefficients for ethanol–water mixtures at various compositions. Nonpolarizable models are used in this study because we are primarily interested in the structure of ethanol at solid–liquid interfaces.

Computational studies of liquid ethanol on solid substrates are somewhat scarce. Andoh and co-workers³⁵ conducted a series of NVT MD calculations for liquid ethanol on a fully hydroxylated silicon dioxide surface. The results showed the formation of molecular clusters of hydrogen-bonded ethanol. Cooke et al.³⁶ investigated ethanol and water on the (10 $\bar{1}$ 4) surface of calcite. A highly ordered adsorbed layer of ethanol was found to be stable even in the presence of water.

Regarding experimental data, Rossetto et al.³⁷ recently studied the impact of ethanol on the adhesion of alumina surfaces in water. They found that the adhesive energy in aqueous solutions decreases as the ethanol concentration increases. The impetus for our work is based on recent experimental data reported by Shen et al.,³⁸ who studied ethanol on the (1 $\bar{1}$ 02) alumina surface using sum frequency vibrational spectroscopy (SFVS). We use equilibrium MD to

Received: December 12, 2012

Revised: February 9, 2013

Published: March 14, 2013

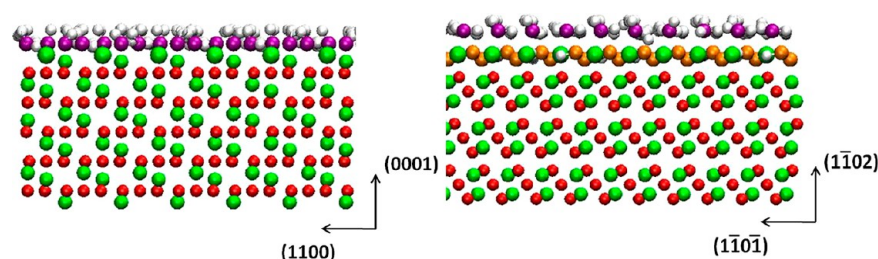


Figure 1. Side view of the fully hydroxylated C-plane (0001) (left) and R-plane ($\bar{1}\bar{1}02$) (right) sapphire surfaces. Green and red spheres represent aluminum and oxygen atoms in the bulk structure, respectively. For the C-plane, surface hydroxyl groups are illustrated using purple for oxygen and white for hydrogen atoms. For the R-plane, surface hydroxyl groups are illustrated using purple for the first oxygen surface layer, orange for the second and third oxygen surface layers, and white for hydrogen atoms. See text for a discussion regarding the different types of OH groups expected on the R-plane.

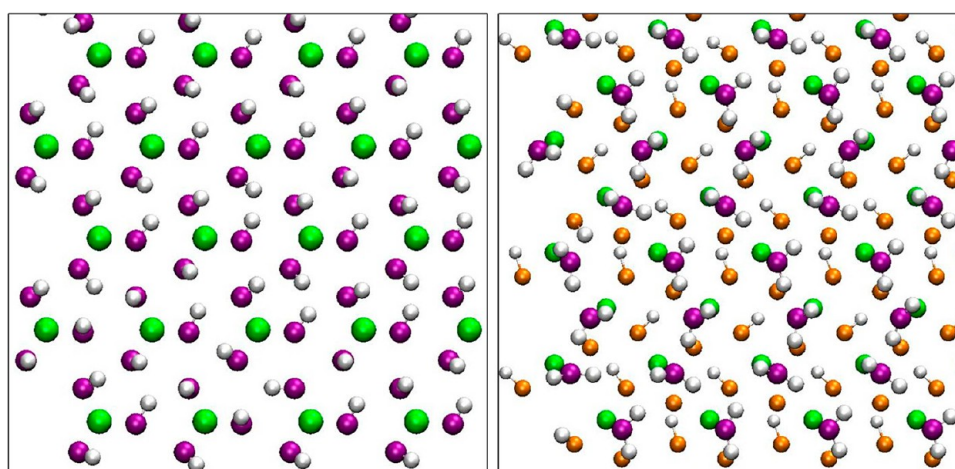


Figure 2. Top view of the surface hydroxyl groups on the (0001) (left) and ($\bar{1}\bar{1}02$) (right) α - Al_2O_3 surfaces. The color scheme for surface hydroxyl groups is the same as that in Figure 1.

study structural and dynamical properties of ethanol within thin liquid films formed on two alumina surfaces—(0001) and ($\bar{1}\bar{1}02$) terminations of the hydroxylated α - Al_2O_3 —at ambient conditions. Good agreement is observed between simulated and experimental data. Quantitative information regarding how the surface features affect adsorbed ethanol via preferential surface–ethanol interactions is discussed.

SIMULATION METHODS AND ALGORITHMS

Two crystallographic faces of sapphire α - Al_2O_3 (space group $R\bar{3}c$)³⁹—C-plane (0001) and R-plane ($\bar{1}\bar{1}02$)—were used to model the alumina surfaces. Both C- and R-plane surfaces are stable termination facets on natural sapphire crystals. Coustet et al.⁴⁰ determined that the C-plane surface is hydroxylated under humid atmospheres. The fully hydroxylated C-plane contains ~ 15 OH groups per square nanometer. Shen et al.⁴¹ investigated the protonated surface structure of the R-plane using sum-frequency vibrational spectroscopy (SFVS). The hydroxylated R-plane⁴² shows three distinct OH species: one H-bonded OH associated with the Al_2OH of the second oxygen surface layer, one H-bonded OH, and one dangling OH associated with the AlOH_2 group of the topmost oxygen layer.⁴¹ Shen et al. suggested that the separation distance between the second and third oxygen surface layers is reduced by ~ 0.55 Å compared with that of the bulk crystal and by ~ 0.3 Å compared with that of the crystal truncation rod (CTR) model.⁴¹ The model implemented herein reflects such recommendations.

In Figure 1 we present the side view of the fully hydroxylated C-plane (0001) (left panel) with the surface normal (0001) and (1100) directions aligned with the Z and Y axis of the simulation box, respectively. We also show the fully hydroxylated R-plane ($\bar{1}\bar{1}02$) (right panel), with the surface normal ($\bar{1}\bar{1}02$) and ($\bar{1}\bar{1}0\bar{1}$) directions aligned with the Z and Y axis of the simulation box, respectively. The top views of both substrates are shown in Figure 2. These are the substrates used in our simulations. The simulations were carried out in orthorhombic simulation boxes of constant volume. The X and Y dimensions of the simulation boxes reflect the periodicity of the solid crystalline substrate with values of 47.6 Å (49.5 Å) and 47.6 Å (46.08 Å) for the C-plane (R-plane). The Z dimension was set to 300 Å for both cases.

A thin ethanol film is prepared along the Z direction, following the procedures of our prior investigations.^{11,13,17,18} See Figure S1 in Supporting Information for a representative simulation snapshot of the simulated system. Using 2000 ethanol molecules, we created a thin film of ~ 94 Å thickness. As the Z dimension of the simulation box was 300 Å, and as the solid substrate thickness of C-plane and R-plane sapphire surfaces were 11.91 and 12.58 Å, respectively, an empty gap exists between the thin film and the periodic image of the solid substrate, as in our prior studies.^{11,17,18}

The CLAYFF force field was implemented to describe both alumina substrates.⁴³ The optimized potential for liquid simulation in the united atom form (OPLS-UA)²⁷ was implemented to describe ethanol. The methyl (CH_3) and

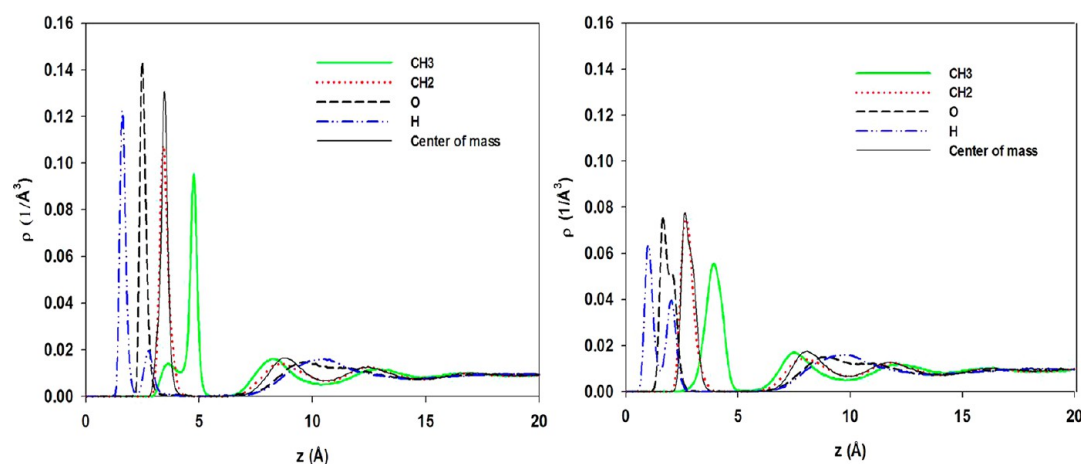


Figure 3. Methyl group (green solid line), ethyl group (red dot line), oxygen (black dash line), and hydrogen (blue double-dot dash line) atomic density profiles of ethanol on the fully hydroxylated C-plane (left) and R-plane α -Al₂O₃ (right) surfaces. In both panels we also report the density profiles for the center of mass of ethanol molecules (black solid lines).

ethyl (CH₂) groups of ethanol are treated within the united-atom formalism. Bond lengths and angles in an ethanol molecule are allowed to oscillate from their equilibrium values, as prescribed by Berkowitz et al.,⁴⁴ by implementing the LINCS algorithm.⁴⁵

Nonbonded interactions were modeled by means of dispersive and electrostatic forces. The electrostatic interactions were modeled by the Coulombic potential. Dispersive interactions were modeled with a 12–6 Lennard-Jones (LJ) potential. The LJ parameters for ethanol–ethanol and ethanol–alumina interactions were determined by geometric mixing rules⁴⁶ from the values of pure components, while the Lorentz–Berthelot mixing rules are used to compute the LJ parameters within the CLAYFF formalism to simulate alumina. The cutoff distance for all interactions was set to 9 Å. Long range corrections to electrostatic interactions were treated using the particle mesh Ewald (PME) method.⁴⁷

All simulations were performed in the canonical ensemble (NVT) where the number of particles (*N*), the simulation volume (*V*), and the temperature (*T*) were kept constant. The simulated temperature was held at 298 K and controlled by a Nosé–Hoover thermostat^{48,49} with a relaxation time of 100 fs. Periodic boundary conditions were applied in all three directions. The simulation package GROMACS^{50,51} was used to solve the equations of motion by implementing the leapfrog algorithm with 1.0 fs time steps. The total simulation time was 25 ns. Data analysis was conducted over the last 5 ns of the simulations after 20 ns of equilibration were completed. Equilibration was achieved when the density of ethanol in the center of the film approached the experimental bulk density at the same thermodynamic conditions.

RESULTS AND DISCUSSION

1. Atomic Density Profiles. Figure 3 reports the atomic density profiles of methyl (CH₃) (green solid line), ethyl (CH₂) (red dot line), oxygen (black dash line), and hydrogen atoms (blue double-dot dash line) of ethanol molecules on the fully hydroxylated C-plane (left panel) and R-plane α -Al₂O₃ (right panel) as a function of the vertical distance. For the C-plane, the reference (*z* = 0) corresponds to the top plane of the hydroxyl group oxygen atoms of the substrate; the reference (*z* = 0) for the R-plane is the plane of the topmost oxygen layer.

The first methyl, ethyl, oxygen, and hydrogen peaks are formed on the C-plane at 4.75, 3.45, 2.45, and 1.65 Å from the surface, respectively. The methyl, ethyl, oxygen and hydrogen peaks within the second layer appear at positions 8.25, 8.55, 9.65, and 10.35 Å, respectively. The results suggest that ethanol molecules found in the first adsorbed layer project their OH groups toward the surface, while they extend their methyl groups toward the bulk liquid. This preferential orientation allows ethanol molecules to form hydrogen bonds with the surface OH groups (according to a geometric criterion, hydrogen bonds can exist when the distance between O and H atoms involved is 1.5–2.1 Å^{52–54}).

The first methyl, ethyl, oxygen, and hydrogen peaks are formed on the R-plane at 3.95, 2.65, 1.65, and 1.05 Å from the surface, respectively. The positions of the methyl, ethyl, oxygen, and hydrogen peaks in the second layer appear at 7.45, 7.75, 8.85, and 9.85 Å, respectively. Even in this case ethanol molecules in the first layer orient their OH bond toward, and the methyl group away from, the surface. The orientation of ethanol molecules within the second layer is opposite that on the first layer.

The atomic density profiles obtained on the two substrates are qualitatively similar to each other. However, the first adsorbed layer on the R-plane is at a slightly shorter distance than that at which the first layer is found on the C-plane. For example, the first hydrogen peaks are observed at 1.05 and 1.65 Å from the two substrates, respectively. This might be a consequence of the choice of reference planes. A smaller methyl group peak within the first layer on the C-plane is also noticed. This peak might not be visible on the R-plane because in the latter the first methyl peak is wider than on the C-plane.

The ethanol hydrogen atoms yield two well-pronounced density peaks near both surfaces. While the second peak at 2.75 Å is very weak on the C-plane, on the R-plane the second peak at 2.05 Å becomes comparable to the first. This probably reflects a different hydrogen-bond network formed on the two substrates. Note also that the density profile for the O atoms of ethanol yields a single, narrow peak on the C-plane, but it yields one peak followed by a pronounced shoulder on the R-plane. It is curious that the density profile for the methyl group shows one peak, albeit wide, on the R-plane, but two peaks (the one closer to the surface much weaker than the other) on the C-plane. This suggests the possibility that excluded-volume effects

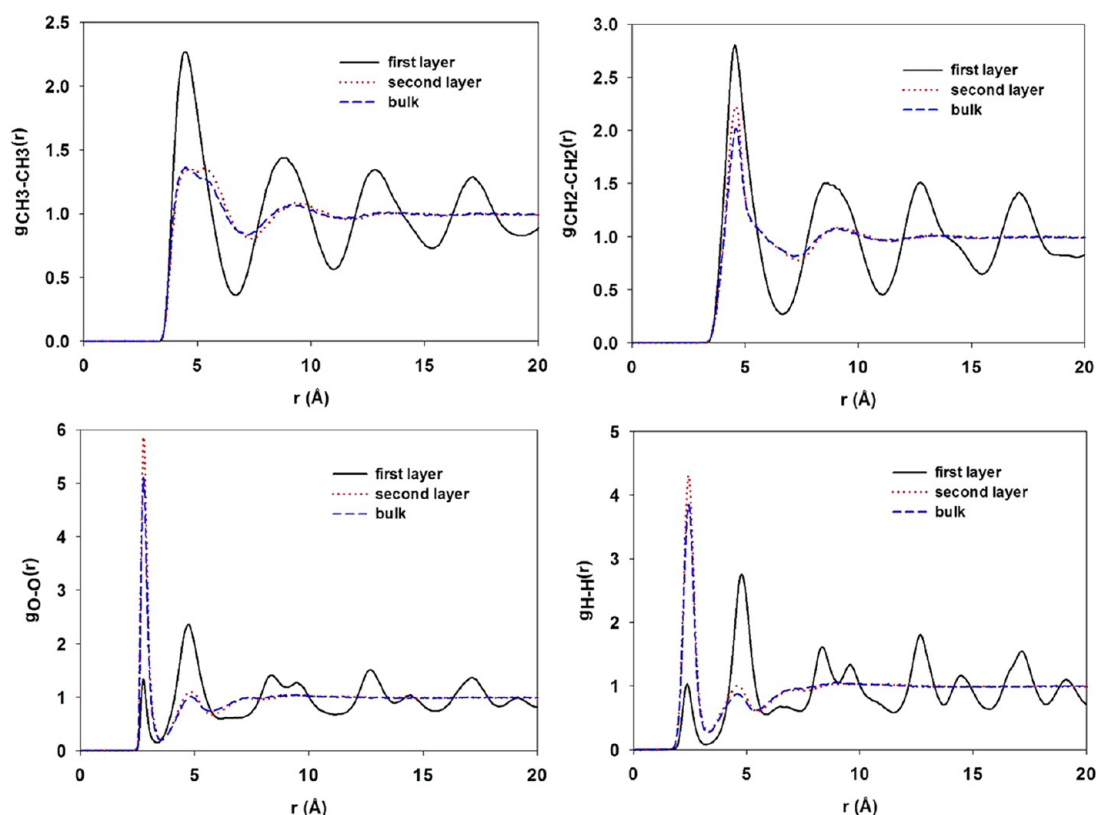


Figure 4. In-plane $\text{CH}_3\text{--CH}_3$ (top left), $\text{CH}_2\text{--CH}_2$ (top right), oxygen–oxygen (bottom left), and hydrogen–hydrogen (bottom right) radial distribution functions for ethanol molecules within various ethanol layers on the alumina C-plane.

might frustrate the packing of ethanol within the first adsorbed layer.

The atomic density profiles indicate the formation of a well-defined first adsorption layer of ethanol on both the C- and R-surfaces, with the ethanol ethyl groups found at 3.45 and 2.65 Å, respectively. The intensity of the density peaks within ~ 7 Å from the R-plane is in general lower than that of the correspondent peaks found on the C-plane. However, the width of the density peaks on the R-plane is wider than that of the corresponding peaks on the C-plane. By integrating the density along the z direction, we confirmed that the number of ethanol molecules found within the first layer on the two substrates per unit surface area is approximately the same.

The density profiles of Figure 3 show evidence for a second layer of ethanol on the C- and R-plane surfaces, formed at vertical positions of 8.55 and 7.75 Å, respectively (positions of the density peak for the ethanol center of mass). Within the second layer, on both substrates, the ethanol methyl group is found closer to the surface than all the other groups of ethanol. This is contrary to what is observed on the first layer, where the ethanol hydrogen atoms are closer to the surface than the methyl groups. It is likely that the OH groups of ethanol in the second layer are effectively repelled from the dense layer formed by the methyl groups of ethanol in the first adsorbed layer. The intensities and the widths of the corresponding density peaks observed on the two substrates are comparable, suggesting that the differences on the surface properties are only felt within the first adsorbed ethanol layer.

The atomic density profiles drop to zero between the first and second adsorption peaks on both substrates. These results are consistent with simulation data reported by Cooke et al.³⁶

and Andoh et al.,³⁵ although these were conducted on calcite and silicon dioxide, respectively.

The atomic density profiles on both surfaces become uniform as the vertical distance approaches 20 Å, suggesting that both alumina substrates perturb interfacial ethanol for up to this distance and that bulk properties are recovered at larger distances. The bulk ethanol density obtained from our simulations is ~ 0.75 g/cm³, consistent with the simulation data reported by Andoh et al.³⁵ and $\sim 4.5\%$ lower than experimental data at the same thermodynamic conditions 298 K and 1 atm (0.785 g/cm³).⁵⁵

To quantify the structure of interfacial ethanol in terms of free energy profiles, we calculated the potential of mean force (PMF) for ethanol as a function of the distance from the surfaces. The results are shown in Figure S2 of the Supporting Information. The PMF data, obtained from the density profiles of the ethanol center of mass,^{36,56} are consistent with those reported for ethanol on the (10 $\bar{1}$ 4) plane of calcite.³⁶ The effective attractive PMF obtained in correspondence to the first adsorbed layer (~ -2.7 and ~ -2.1 kT on C- and R-plane, respectively) is due in part to the propensity of the ethanol molecules to form hydrogen bonds with the hydroxyl groups available on both surfaces. In correspondence to the depleted layer in between first and second adsorbed layers, our PMF results show a significant repulsive barrier (~ 6.3 and ~ 5.0 kT for C-plane and R-plane, respectively). The presence of this significant free-energy barrier suggests that ethanol molecules adsorbed within the first adsorbed layer are rarely able to exchange with molecules further from the surface, as confirmed below.

2. In-Plane Radial Distribution Functions. In-plane radial distribution functions (RDFs) were calculated between

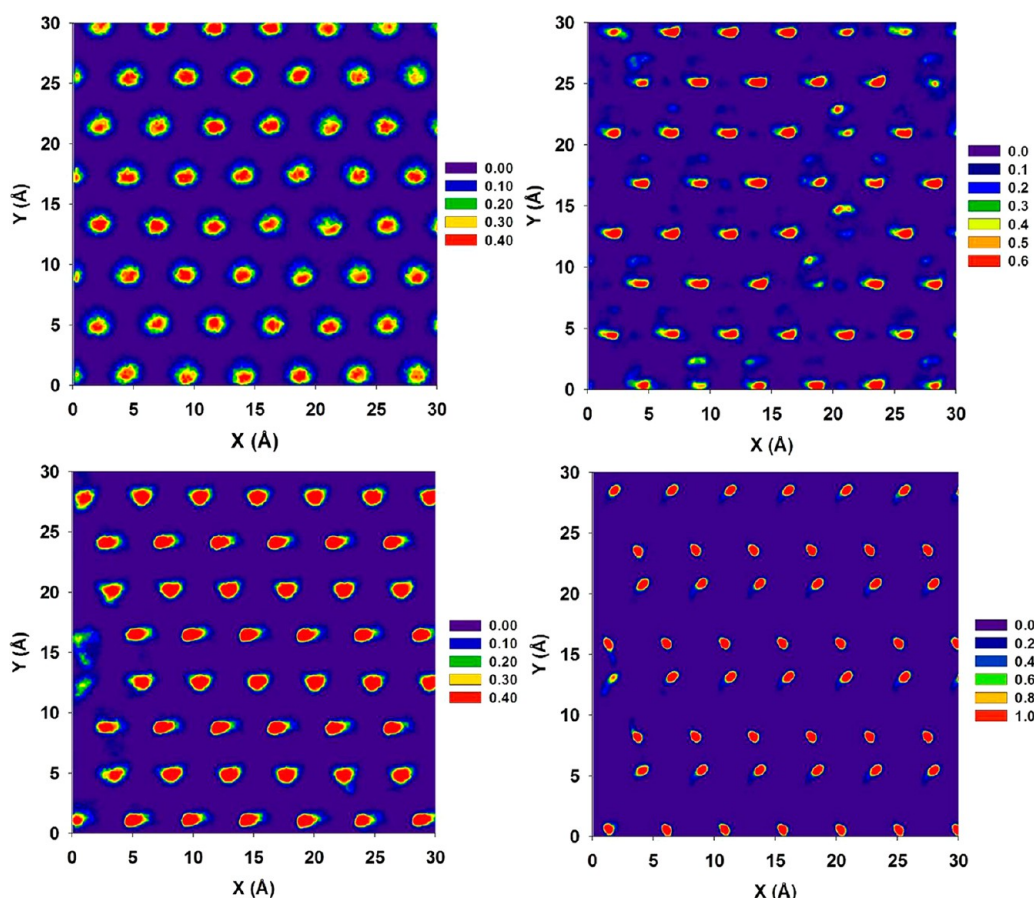


Figure 5. In-plane density distributions of CH₃ groups (left panel) and O atoms (right panel) of ethanol molecules within the first adsorbed layer on the α -Al₂O₃ C- (top) and R-plane (bottom). Densities are expressed in 1/Å³.

CH₃–CH₃, CH₂–CH₂, oxygen–oxygen, and hydrogen–hydrogen of ethanol molecules to quantify the structural properties within the various adsorbed layers. Results are compared to those obtained in the bulk (i.e., far from the surfaces). For these calculations, following our prior algorithms,^{13,16} only ethanol molecules found within a given slab parallel to the surface were considered. The thickness (δz) of the slab was 5 Å for the calculations shown here. Bulk ethanol is identified as ethanol found at $z > 20$ Å from the substrates.

In Figure 4, the results are presented for in-plane RDFs for ethanol in the first and second layers on the C-plane. Several pronounced peaks are observed in all RDFs within the first layer, suggesting a well-ordered molecular structure. The results obtained in the second layer, as well as those obtained for bulk ethanol, are indicative of liquid structures with no pronounced order. These results indicate that C-plane alumina only perturbs the first adsorbed layer of ethanol (up to distances shorter than ~ 6 Å). This is surprising when compared to the results for the polar orientation, discussed in Figure 3, which show ordered structure up to ~ 10 – 12 Å from the surface.

The most pronounced peak of all in-plane RDFs in the first layer on the C-plane is located at ~ 5 Å. This distance corresponds to the first peak for $g_{\text{CH}_3\text{-CH}_3}(r)$ and $g_{\text{CH}_2\text{-CH}_2}(r)$, and to the second peak for $g_{\text{OO}}(r)$ and $g_{\text{HH}}(r)$. The results obtained within the second layer and in the bulk show that the most pronounced peak of the RDFs always corresponds to the first peak (found at 5 Å for methyl–methyl and ethyl–ethyl RDFs, but at shorter distances for O–O and H–H RDFs). This suggests that while in the bulk both the interactions between

methyl and ethyl groups and those between the hydroxyl groups are responsible for determining the liquid structure, in the first layer steric effects (dictated by methyl–methyl and ethyl–ethyl interactions) assume a dominant role. The interactions between the hydroxyl groups of ethanol molecules are not as important as they are in the bulk because, as shown below, such groups interact preferentially with the solid substrate, rather than with other ethanol molecules.

The results for in-plane $g_{\text{CH}_3\text{-CH}_3}(r)$, $g_{\text{CH}_2\text{-CH}_2}(r)$, $g_{\text{OO}}(r)$, and $g_{\text{HH}}(r)$ for ethanol on the R-plane are shown in Figure S3 of the Supporting Information. Despite some differences due to the different packing of ethanol within the first adsorbed layer, the results are consistent with those found on the C-plane.

3. In-Plane Density Distributions. To visualize the organization of adsorbed ethanol molecules, we calculated the in-plane density distributions of methyl, ethyl, oxygen, and hydrogen of ethanol molecules within the first adsorbed layer. The results are shown in Figure 5 for CH₃ groups (left) and oxygen atoms (right) of ethanol on the C-plane (top panels) and R-planes (bottom panels). The complete sets of results are shown in Figures S4 and S5 of the Supporting Information. In general, on both substrates the in-plane distribution of the methyl groups is representative of the in-plane distribution of CH₂ groups, while that of O atoms is representative of that of H atoms. Because the results above suggest disordered liquid structure for ethanol molecules within the second layer, only ethanol molecules within the first layer were used for the present calculations.

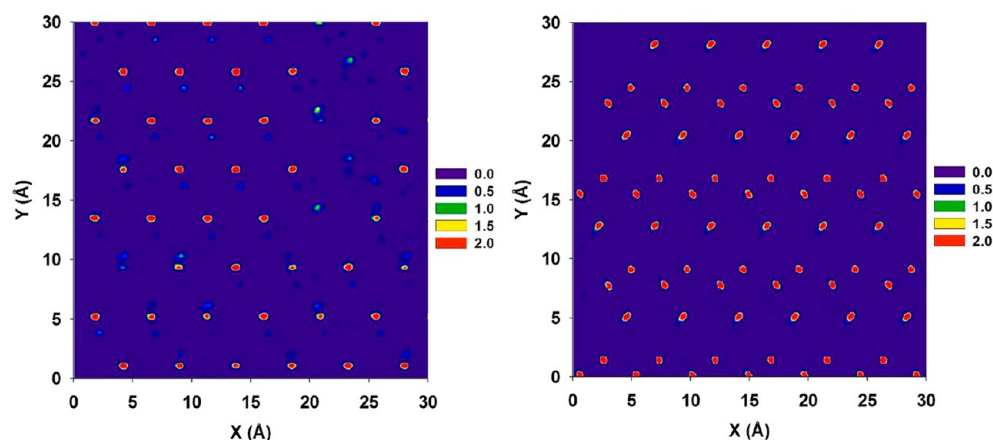


Figure 6. In-plane density distribution of hydrogen bonds formed between ethanol molecules in the first adsorbed layer and the hydroxyl groups present on the C- (left panel) and R-plane (right panel). Densities are expressed in $1/\text{\AA}^3$.

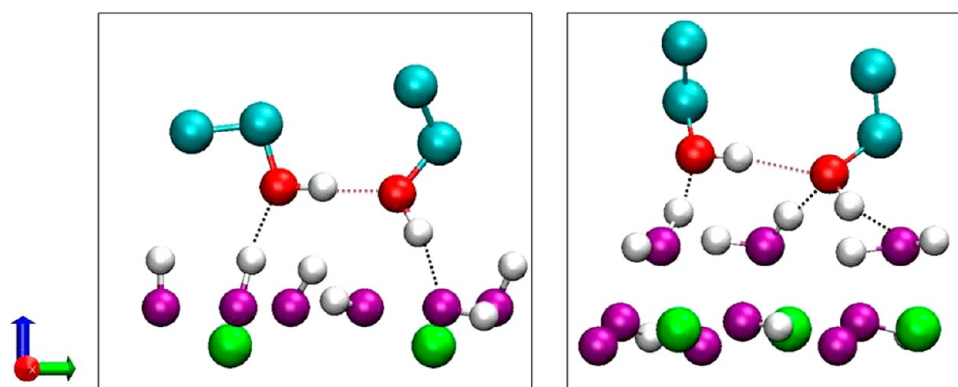


Figure 7. Simulation snapshots of selected ethanol molecules in the first adsorbed layer on the C- (left) and the R-planes (right). Only a few atomic surface hydroxyl groups are shown for clarity. The first adsorbed layer of ethanol is defined by those ethanol molecules whose center of mass is found at vertical distances less than 5 Å from the substrate (see density profiles). Cyan, red, and white spheres represent alkyl groups, oxygen, and hydrogen atoms of ethanol molecules, respectively. Surface hydroxyl groups are shown with green, purple, and white spheres for aluminum, oxygen, and hydrogen atoms, respectively. Black dot lines represent the H-bonds formed between ethanol molecules and the surface OH groups. Red dot lines represent the H-bonds formed between ethanol molecules. Note that, in agreement with the density profiles, the oxygen atoms of ethanol are found closer to the topmost layer of oxygen atoms of the R-plane (right) than to those of the C-plane (left).

The results in Figure 5 suggest that ethanol molecules occupy specific adsorption sites on each of the alumina surfaces. The resulting structures show high degrees of order, which is consistent with the in-plane radial distribution functions discussed above. Some differences can be observed between the two substrates. On the C-plane the distance between each preferential adsorption site is ~ 5 Å (consistent with RDF results), whereas the distance between surface hydroxyl groups is ~ 2.5 Å. It is likely that the size of ethanol molecules prevents them from interacting with all hydroxyl groups available on the substrate. Also on the R-plane the minimum distance between two methyl preferential adsorption sites is ~ 5 Å. However, next neighboring preferential adsorption sites for O atoms on the R-plane are located at distances of both ~ 2.5 and ~ 5 Å.

To visualize the structure of the adsorbed ethanol, in Figure S6 of the Supporting Information, we report top and side views of representative simulation snapshots obtained for ethanol on the C- and on the R-plane. The snapshots reconcile why the preferential adsorption sites for all ethanol groups on the C-plane yield hexagonal patterns, while on the R-plane CH_3 and CH_2 groups yield hexagonal structures but O and H atoms do not. These differences are due to different hydrogen bond

networks formed between adsorbed ethanol and the solid substrates, as discussed in the next section.

4. Hydrogen Bond Network. To relate the distribution of ethanol in the first adsorbed layer to that of the surface hydroxyl groups, we calculated the density distribution of hydrogen bonds formed between the surface OH groups and ethanol on both the C- and R-planes. A geometric criterion was used to identify one hydrogen bond. According to this criterion a hydrogen bond is formed when the angle $\text{OH}\cdots\text{O}$ is larger than 150° and the $\text{O}\cdots\text{H}$ distance is between 1.5 and 2.1 Å.^{52–54} The results, shown in Figure 6, suggest that while on the C-plane many surface–ethanol hydrogen bonds form in locations correspondent to the preferential adsorption of oxygen and hydrogen atoms of ethanol (compare the left panel of Figure 6 to the top right panel of Figure 5), the same is not necessarily observed on the R-plane (compare the right panel of Figure 6 to the bottom right panel of Figure 5). Visualizing representative simulation snapshots (Figure 7), we confirm that these differences occur because on the C-plane each adsorbed ethanol forms one hydrogen bond with one surface hydroxyl group. On the R-plane one adsorbed molecule can form one hydrogen bond with one OH group, but also two hydrogen bonds with two neighboring surface OH groups.

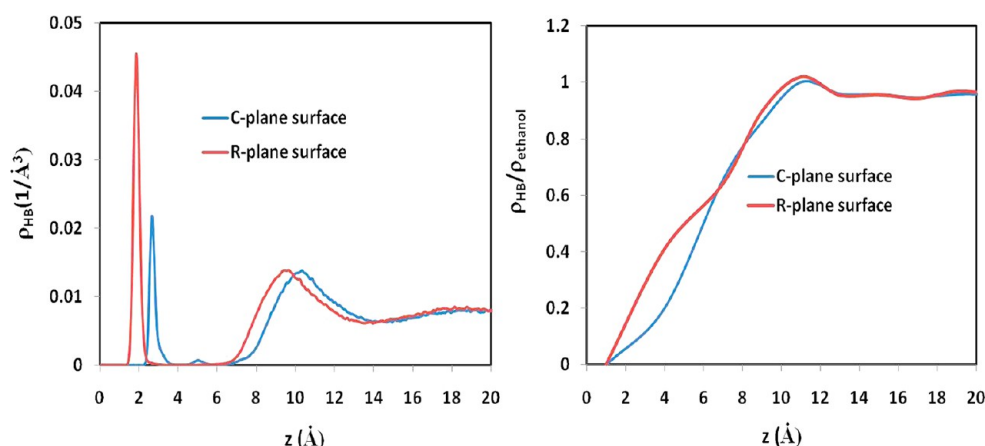


Figure 8. Left: Density profiles of ethanol–ethanol hydrogen bonds as a function of the distance z from the C- (blue) and R-plane (red). Right: Ratio between the density of ethanol–ethanol hydrogen bonds to that of ethanol molecules as a function of the distance z from both substrates.

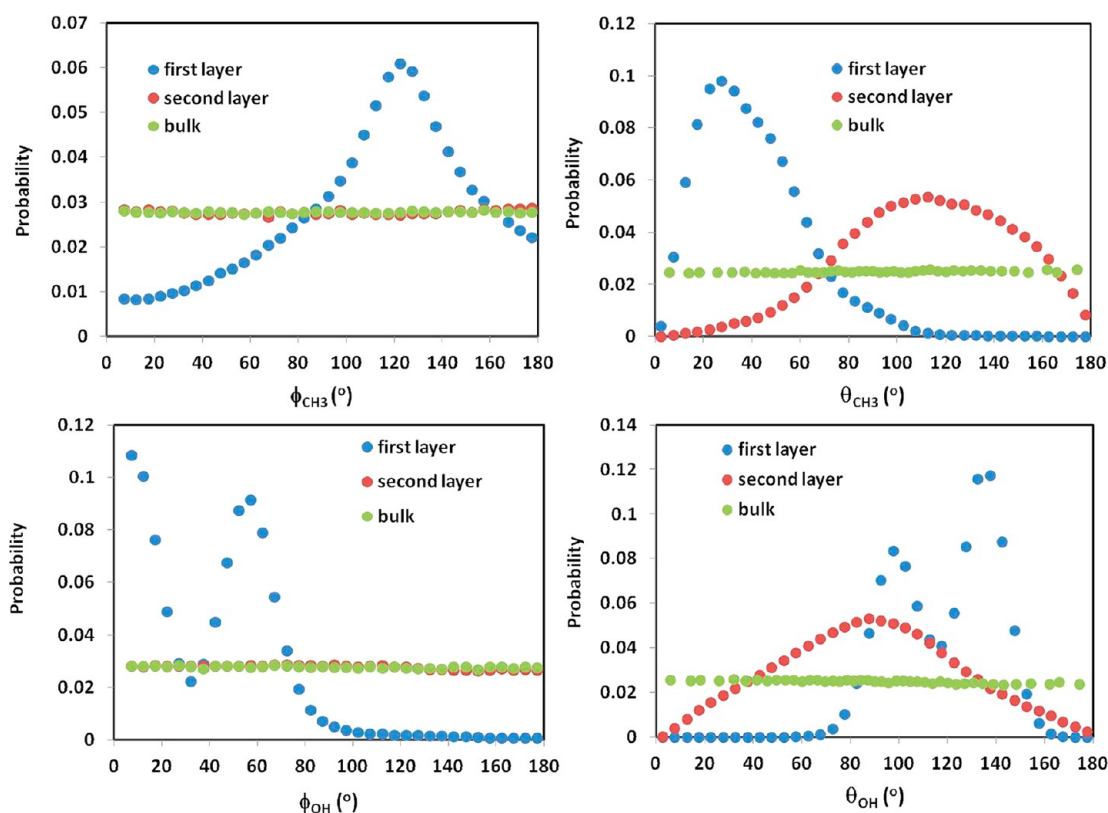


Figure 9. Probability distribution for ϕ_{CH_3} (top left panel), θ_{CH_3} (top right panel), ϕ_{OH} (bottom left panel), and θ_{OH} (bottom right panel) in the first and second layers, as well as in the bulk. ϕ_{CH_3} and ϕ_{OH} are the azimuthal angles of the symmetry axis of the methyl CH_3 group and of the OH groups with respect to the (1101) direction, respectively. θ_{CH_3} and θ_{OH} are the polar angles with respect to the surface normal (see Figure S7 for schematic).

These OH groups are found in correspondence to two different relative positions with respect to the surface $AlOH_2$ groups.

Our results also show that the density of hydrogen bonds formed between ethanol and the R-plane (~ 0.07 H-bonds per Å^2) is greater than that of hydrogen bonds formed between ethanol and the C-plane (~ 0.05 H-bonds per Å^2).

In Figure 8 we report the density profile of ethanol–ethanol hydrogen bonds as a function of the distance z from the C- and R-plane. The most important observation is that many ethanol–ethanol hydrogen bonds form between molecules found in the first layer adsorbed on both substrates (data more evident on the R-plane). This result is at first sight surprising,

given the discussion concerning ethanol–surface hydrogen bonds. However the two-dimensional RDFs (see Figure 4) suggest that the positions of the first peak in both O–O and H–H profiles are at distances comparable to those observed in the bulk, although their intensity is significantly lower. The simulation snapshots (Figure 7) show that the well-ordered ethanol molecules within the first adsorbed layers can form ethanol–ethanol hydrogen bonds. To quantify the ability of ethanol molecules to form hydrogen bonds with other ethanol molecules as a function of the distance from the interface, we calculated the ratio between the density of ethanol–ethanol hydrogen bonds and that of ethanol molecules at each position.

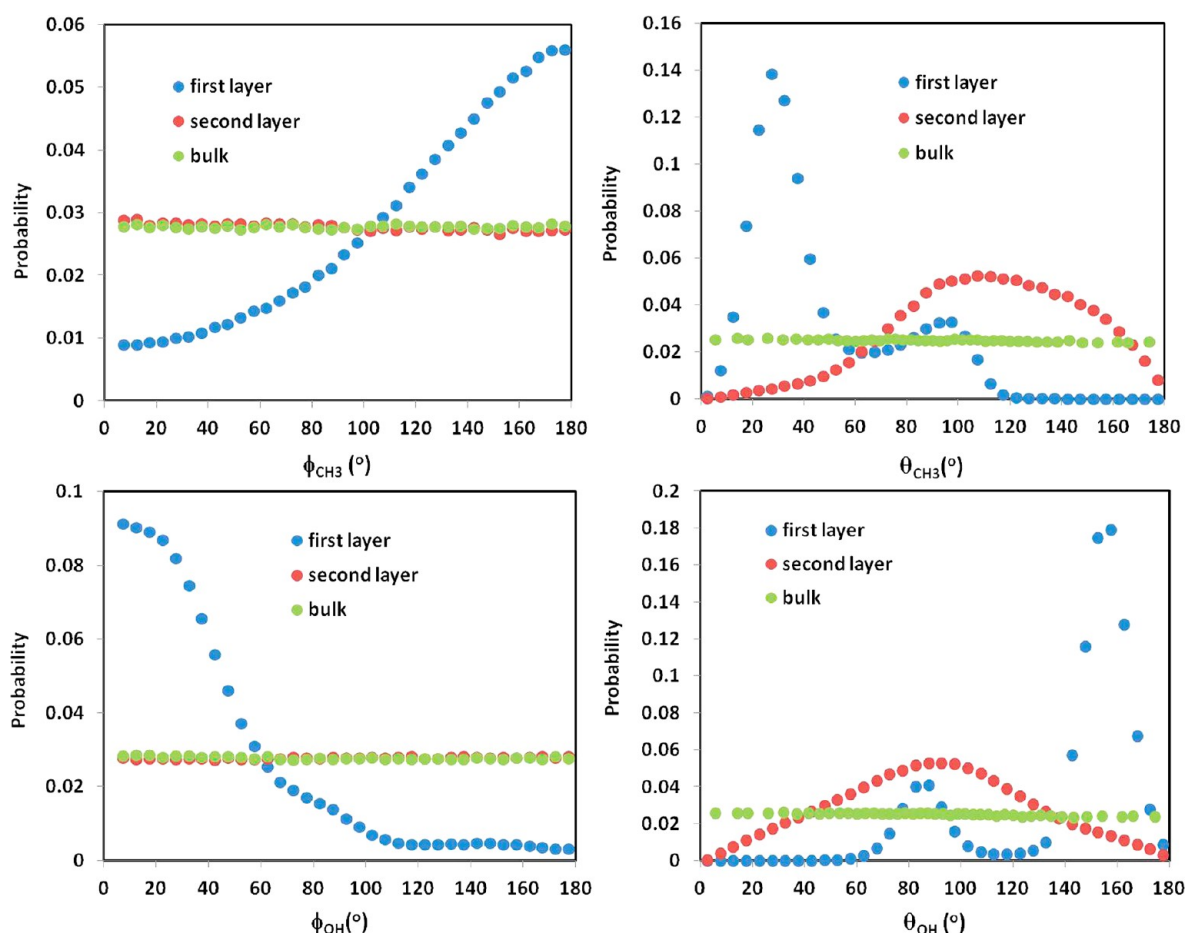


Figure 10. Same as Figure 9, for ethanol on the *R*-plane.

The results are shown in the right panel of Figure 8. Near both surfaces the ratio is less than 1, and it increases to unity at large separations. We conclude that each ethanol in the bulk forms two hydrogen bonds with other ethanol molecules (one as donor, one as acceptor), while one out of every three ethanol molecules is engaged via hydrogen bonds with other ethanol molecules near the *R*-plane (one out of six near the *C*-plane). Ethanol molecules within the adsorbed layer prefer to form hydrogen bonds with the surface OH groups. This behavior contrasts that of water, for which our simulations on the *C*-plane suggest the possibility of forming numerous water–water HBs, in addition to water–surface ones.^{16,18}

5. Ethanol Orientation. We computed azimuthal and polar angles of the symmetric axis of the methyl group and of the OH group of each ethanol molecule with respect to the (1 $\bar{1}$ 0 $\bar{1}$) direction and the surface normal (1 $\bar{1}$ 02) (*R*-plane), or the (1100) direction and the surface normal (0001) (*C*-plane), as described pictorially in Figure S7 of the Supporting Information. The symmetric axis of the methyl group connects CH₃ and CH₂ in one ethanol molecule.

We begin the discussion with the *R*-plane, because experimental data are available to validate our predictions. The probability distribution of azimuthal and polar angles for the methyl and the OH symmetry axis are shown in Figure 9, top and bottom panels, respectively. We point out that it is difficult to determine the orientation of the ethanol vector \overline{OH} within the first layer by experimental sum frequency vibrational spectroscopy (SFVS), as discussed by Shen et al.³⁸ Such

information can however be extracted from our simulations to complement the experimental observations. We report the results obtained for ethanol molecules in the first and second adsorbed layers, as well as for bulk ethanol. Ethanol molecules in the first layer orient such that the azimuthal angle for the symmetry axis of the methyl group is preferentially $\sim 125 \pm 5^\circ$ and the polar angle $\sim 28 \pm 5^\circ$. These data compare well with the experimental values reported by Shen et al.³⁸ These authors employed SFVS to sample the orientation of a monolayer of ethanol at the *R*-plane–air interface. The results were consistent with azimuthal and polar angles of $\sim 132 \pm 8^\circ$ and $\sim 38 \pm 7^\circ$, respectively. When the experiments were repeated for liquid ethanol at the *R*-plane interface, the results still showed a strongly oriented first adsorbed layer with similar orientations (with ethanol orientation consistent with the one observed for the monolayer case) and an ordered second adsorbed layer. Thermal motion was found to affect the second layer much more than the first. Considering that in our simulations ethanol molecules in the first adsorbed layer interact with those in the second layer, agreement with experiments appears satisfactory.

Regarding the orientation of the OH group, in the first layer its azimuthal angle is found to be preferentially $\sim 5^\circ$ and $\sim 58^\circ$, while the polar angle is preferentially $\sim 138^\circ$ and $\sim 98^\circ$. These two peaks are representative of the two structures of ethanol–surface hydrogen bonds, shown in Figure 7.

The azimuthal orientation of both methyl and OH groups of ethanol molecules in the second adsorbed layer is similar to that found in the bulk. However, the polar orientation of the

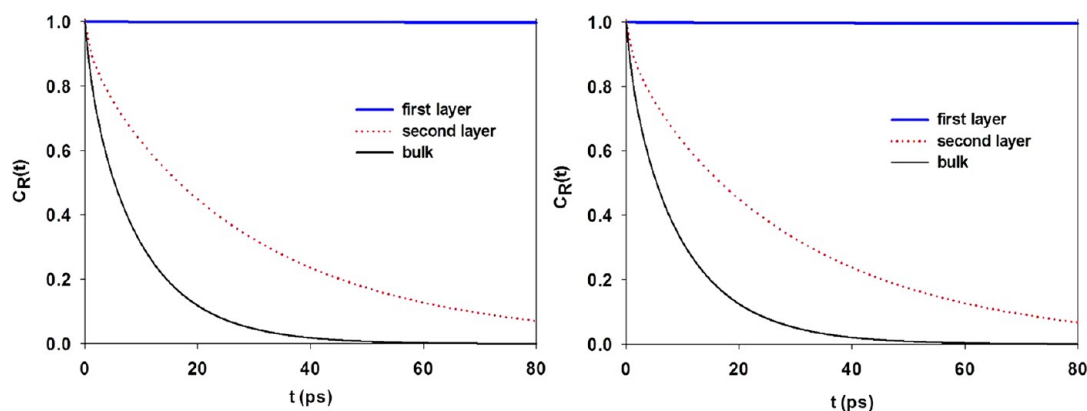


Figure 11. Residence autocorrelation functions $C_R(t)$ for the ethyl group of ethanol molecules within the first (blue solid line) and second adsorbed layers (red dot line). Data obtained in the bulk are shown for comparison (black solid line). Results are shown for ethanol on the C-plane (left panel) and on R-plane (right panel), respectively.

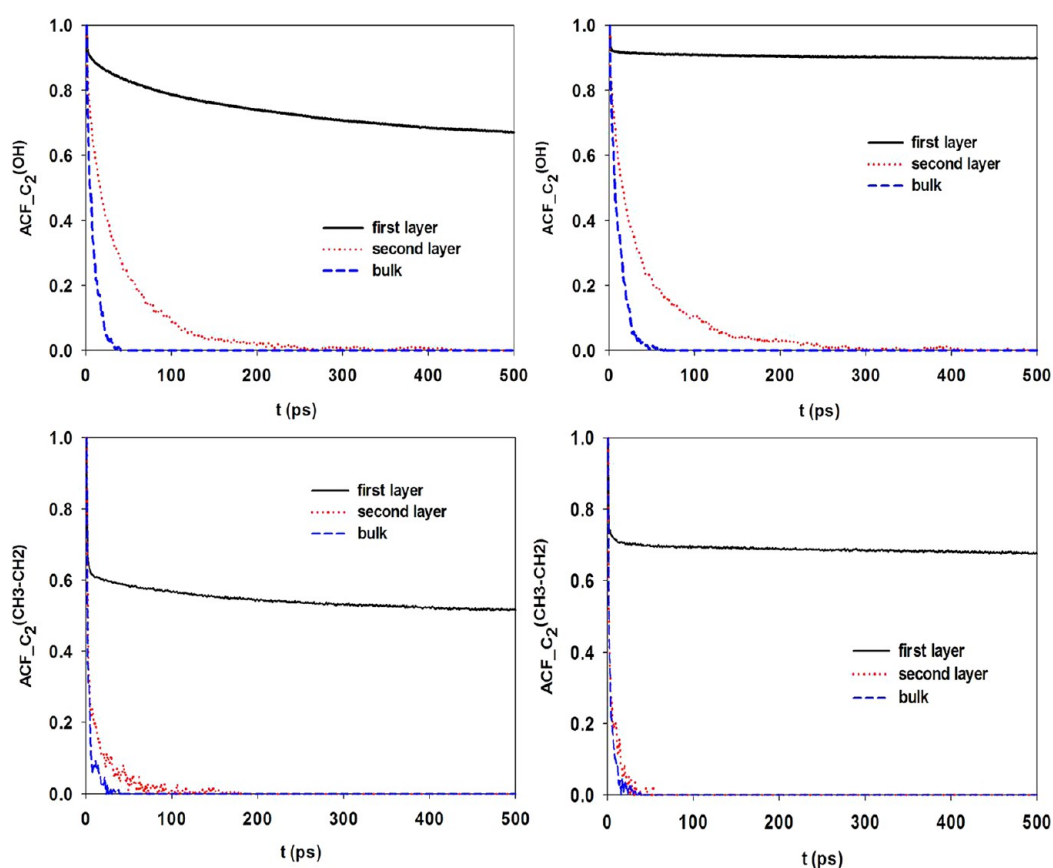


Figure 12. Top: Reorientation autocorrelation functions for OH group of ethanol molecules within the first (black solid line) and second adsorbed layers (red dot line). Bottom: Reorientation autocorrelation functions of the symmetry axis of the methyl CH_3 group of ethanol molecules within the first (black solid line) and second adsorbed layers (red dot line).

symmetry axis of the methyl CH_3 group with respect to the surface normal ($1\bar{1}02$) in the second layer shows preference for a polar angle at $\sim 113^\circ$. The polar orientation of the OH group in the second layer is also different compared to that found in the first adsorbed layer. These differences reflect the fact that ethanol molecules in the first adsorbed layer project their OH group toward the surface, while those in the second layer project the OH group away from the surface, as discussed above (see Figure 3).

In Figure 10 we present the results for the orientation of ethanol molecules adsorbed on the C-plane. Different

orientations compared to those discussed on the R-plane are clearly evident. For example the symmetry axis of the methyl groups in the first layer preferentially point along the backward direction with respect to the (1100) vector. The probability distribution for the polar orientation of the methyl symmetry axis for ethanol in the first layer shows two preferential orientations, $\sim 28^\circ$ and $\sim 98^\circ$. Consistent with the density distributions of Figure 3, these data suggest that the symmetry axis of the methyl group points away from the C-plane, with a slight probability of maintaining the methyl symmetry axes parallel to the substrate. Ethanol molecules in the second layer

do not show a preferential azimuthal orientation for the methyl symmetry axis, while the polar angles show a preference at $\sim 113^\circ$.

Results for the preferential orientation of the \overline{OH} vector of ethanol suggest that also on the C-plane this vector either points toward the surface or remains approximately parallel to it. The results obtained in the second layer suggest a different orientation, with many OH bonds parallel to the surface. These data are similar to those obtained on the R-plane.

6. Dynamical Properties. To quantify how long ethanol molecules remain in contact with the alumina surfaces, we computed the residence autocorrelation function $C_R(t)$ within first and second adsorbed layers (for a discussion on the method, see ref 11). The faster the autocorrelation function decays to 0, the shorter the ethanol molecules stay in a specific hydration layer. The thickness of one layer was considered to be 5 Å. For comparison, we also computed the residence autocorrelation function for ethanol molecules in a layer far from the surface (i.e., “bulk ethanol”). We computed $C_R(t)$ for methyl, ethyl, oxygen, and hydrogen belonging to ethanol. The results were statistically identical, and only results for CH_2 are shown in Figure 11. In the left and right panels we show results obtained on the C- and R-plane, respectively.

The results suggest that ethanol molecules adsorbed in the first layer do not leave either substrate within the 80 ps of the analysis ($C_R(t)$ was calculated in the first layer on both substrates for up to 2 ns, and very slow decay was observed). The ethanol molecules in the second layer are much more mobile compared to those in the first layer, but they show a much longer residence time than ethanol molecules in the bulk. Based on results for density profiles and surface–ethanol potential of mean force, it was expected that ethanol molecules would remain at contact with the two substrates for very long times. It was however not obvious that ethanol molecules in the second layer would also show reduced exchange rate with ethanol molecules in the bulk. This might be due to the fact that ethanol molecules in the first adsorbed layers provide a very tight structure, on which ethanol molecules form a second adsorbed layer.

To quantify the rotational dynamics of ethanol molecules as a function of the distance from the substrate, we calculated the reorientation autocorrelation function:⁵⁷

$$C_\nu(t) = \frac{\langle \nu(t) \nu(0) \rangle}{\langle \nu(0) \nu(0) \rangle} \quad (1)$$

In eq 1 ν is either the vector \overline{OH} or the symmetric axis of the methyl group of one ethanol molecule. The faster the ACF decays to zero, the more quickly ethanol molecules change their orientation. Ethanol molecules in the first and second adsorbed layers are considered and compared in Figure 12 to results obtained for bulk ethanol. The results are shown for ethanol on the C- (left) and R-plane (right). As expected, on both surfaces our results suggest that ethanol molecules in the first layer rotate more slowly than those in the second layer and much more slowly than those in the bulk. We note that in the first layer the symmetry axis of methyl group changes its orientation faster than the vector \overline{OH} . This is due to the hydrogen bonds between ethanol and the surfaces, which are difficult to break and thus slow down the OH rotation. We also note that both rotational ACFs for ethanol in the first adsorbed layer on either substrate decay much faster than the residence autocorrelation function in Figure 11. This suggests that hydrogen bonds form

and break more frequently than ethanol molecules leave the first adsorbed layer.

Both rotational ACFs decay more slowly for ethanol molecules within the first adsorbed layer on the R-plane than on the C-plane. This is probably related to the higher density of ethanol–surface HBs detected on the R-plane. Results on the second layer are not significantly different on the two substrates.

Although the structure of ethanol molecules in the second adsorbed layer is for the most part similar to that observed for bulk ethanol (except for its preferential orientation), results for the dynamics show that the residence time of ethanol molecules within this layer is much longer than that in the bulk and that the orientational diffusion is slightly slower than that observed in the bulk.

CONCLUSIONS

Molecular dynamics simulations were conducted to study structure and dynamics of liquid ethanol within thin films supported on the C-plane and R-plane alumina surfaces at ambient conditions. The results show that ethanol molecules in the first adsorbed layer have a pronounced order, reflecting the structure of the substrates and the possibility of forming hydrogen bonds with the surface OH groups. A significant orientational order is observed within the first adsorbed layer on both surfaces with the methyl groups preferentially projecting toward the bulk and the OH groups forming hydrogen bonds with both the solid substrates and other ethanol molecules (to a much lesser extent). The preferential orientation of ethanol molecules within the first adsorbed layer on the R-plane is consistent with experimental sum frequency vibrational spectroscopy data. Also consistently with experiments, we found that ethanol molecules show some order within the second adsorbed layer, but to a much lesser extent compared to results obtained for ethanol in the first adsorbed layer on both C- and R-planes. Our results suggest that those molecules in the first adsorbed layer seldom leave, and that their rotational diffusion is hindered compared to bulk values, probably because of preferential hydrogen bonds with the substrates. As suggested by Catalano et al. in the case of water,^{58–60} our results can be explained by the formation of a complex hydrogen-bonded network between adsorbed ethanol and the supporting solid substrates. The results presented here could be useful to advance our understanding regarding the behavior of hydrogen-bonding and amphiphilic molecules in contact with materials of both technological and geological importance. Applications that could benefit from this understanding include industrial, geophysical, petroleum, and environmental ones.

ASSOCIATED CONTENT

Supporting Information

Details of force-field parameters and combining rules implemented in this work, schematics for the simulated systems and for the orientation of interfacial ethanol, and results for free-energy profiles, radial distribution functions, in-plane density distributions, and representative simulation snapshots. This material is available free of charge via the Internet at <http://pubs.acs.org>.

AUTHOR INFORMATION

Corresponding Author

*E-mail: astriolo@ou.edu.

Notes

The authors declare no competing financial interest.

ACKNOWLEDGMENTS

A.P. and A.S. were supported by the U.S. Department of Energy, Office of Basic Energy Sciences, under Contract Number DE-SC0006901 (Division of Chemical Sciences, Geosciences, and Biosciences). D.R.C. was supported under contract DE-SC0006878 provided by the U.S. Department of Energy, Office of Basic Energy Sciences (Division of Chemical Sciences, Geosciences, and Biosciences). Partial support was also provided by the Sloan Foundation, via the Deep Carbon Observatory initiative. Generous allocations of computing time were provided by the Oklahoma Supercomputer Center for Education and Research (OSCER) and by the National Energy Research Scientific Computing Center (NERSC). NERSC is supported by the DoE Office of Science under Contract No. DE-AC02-05CH11231.

REFERENCES

- (1) Fornasiero, F.; Park, H. G.; Holt, J. K.; Stadermann, M.; Grigoropoulos, C. P.; Noy, A.; Bakajin, O. Ion Excursion by Sub-2-nm Carbon Nanotube Pores. *Proc. Natl. Acad. Sci. U.S.A.* **2008**, *105*, 17250–17255.
- (2) Hille, B. *Ion Channels of Excitable Membranes*, 3rd ed.; Sinauer Associates, Inc.: Sunderland, MA, 2001.
- (3) Jiang, Y.; Lee, A.; Chen, J.; Cadene, M.; Chait, B. T.; MacKinnon, R. Crystal Structure and Mechanism of a Calcium-Gated Potassium Channel. *Nature* **2002**, *417*, 512–522.
- (4) Argyris, D.; Cole, D. R.; Striolo, A. Ion-Specific Effects under Confinement: The Role of Interfacial Water. *ACS Nano* **2010**, *4*, 2035–2042.
- (5) Ho, T. A.; Argyris, D.; Cole, D. R.; Striolo, A. Aqueous NaCl and CsCl Solutions Confined in Crystalline Slit-Shaped Silica Nanopores of Varying Degree of Protonation. *Langmuir* **2012**, *28*, 1256–1266.
- (6) Malikova, N.; Cadene, A.; Marry, V.; Dubois, E.; Turq, P. Diffusion of Water in Clays on the Microscopic Scale: Modeling and Experiment. *J. Phys. Chem. B* **2006**, *110*, 3206–3214.
- (7) Mamontov, E.; Wesolowski, D. J.; Vlcek, L.; Cummings, P. T.; Rosenqvist, J.; Wang, W.; Cole, D. R. Dynamics of Hydration Water on Rutile Studied by Backscattering Neutron Spectroscopy and Molecular Dynamics Simulation. *J. Phys. Chem. C* **2008**, *112*, 12334–12341.
- (8) Fenn, E. E.; Wong, D. B.; Fayer, M. D. Water Dynamics at Neutral and Ionic Interfaces. *Proc. Natl. Acad. Sci. U.S.A.* **2009**, *106*, 15243–15248.
- (9) Skelton, A. A.; Fenter, P.; Kubicki, J. D.; Wesolowski, D. J.; Cummings, P. T. Simulations of the Quartz(10 $\bar{1}$ 1)/Water Interface: A Comparison of Classical Force Fields, Ab Initio Molecular Dynamics, and X-ray Reflectivity Experiments. *J. Phys. Chem. C* **2011**, *115*, 2076–2088.
- (10) Kerisit, S.; Liu, C. X.; Ilton, E. S. Molecular Dynamics Simulations of the Orthoclase (001)- and (010)-Water Interfaces. *Geochim. Cosmochim. Acta* **2008**, *72*, 1481–1497.
- (11) Argyris, D.; Tummala, N. R.; Striolo, A.; Cole, D. R. Molecular Structure and Dynamics in Thin Water Films at the Silica and Graphite Surfaces. *J. Phys. Chem. C* **2008**, *112*, 13587–13599.
- (12) Giovambattista, N.; Rossky, P. J.; Debenedetti, P. G. Effect of Temperature on the Structure and Phase Behavior of Water Confined by Hydrophobic, Hydrophilic, and Heterogeneous Surfaces. *J. Phys. Chem. B* **2009**, *113*, 13723–13734.
- (13) Argyris, D.; Cole, D. R.; Striolo, A. Hydration Structure on Crystalline Silica Substrates. *Langmuir* **2009**, *25*, 8025–8035.
- (14) Wang, J. W.; Kalinichev, A. G.; Kirkpatrick, R. J. Asymmetric Hydrogen Bonding and Orientational Ordering of Water at Hydrophobic and Hydrophilic Surfaces: A Comparison of Water/Vapor, Water/Talc, and Water/Mica Interfaces. *J. Phys. Chem. C* **2009**, *113*, 11077–11085.
- (15) Kalra, A.; Garde, S.; Hummer, G. Osmotic Water Transport Through Carbon Nanotube Membranes. *Proc. Natl. Acad. Sci. U.S.A.* **2003**, *100*, 10175–10180.
- (16) Phan, A.; Ho, T. A.; Cole, D. R.; Striolo, A. Molecular Structure and Dynamics in Thin Water Films at Metal Oxide Surfaces: Magnesium, Aluminum, and Silicon Oxide Surfaces. *J. Phys. Chem. C* **2012**, *116*, 15962–15973.
- (17) Ho, T. A.; Argyris, D.; Papavassiliou, D. V.; Cole, D. R.; Striolo, A. Interfacial Water on Crystalline Silica: A Comparative Molecular Dynamics Simulation Study. *Mol. Simul.* **2011**, *37*, 172–195.
- (18) Argyris, D.; Ho, T. A.; Cole, D. R.; Striolo, A. Molecular Dynamics Studies of Interfacial Water at the Alumina Surface. *J. Phys. Chem. C* **2011**, *115*, 2038–2046.
- (19) Skelton, A. A.; Wesolowski, D. J.; Cummings, P. T. Investigating the Quartz (10 $\bar{1}$ 1)/Water Interface using Classical and Ab Initio Molecular Dynamics. *Langmuir* **2011**, *27*, 8700–8709.
- (20) Saiz, L.; Padro, J. A.; Guardia, E. Structure and Dynamics of Liquid Ethanol. *J. Phys. Chem. B* **1997**, *101*, 78–86.
- (21) Gao, J. L.; Habibollahzadeh, D.; Shao, L. A Polarizable Intermolecular Potential Function for Simulation of Liquid Alcohols. *J. Phys. Chem.* **1995**, *99*, 16460–16467.
- (22) Saiz, L.; Guardia, E.; Padro, J.-A. Dielectric Properties of Liquid Ethanol. A Computer Simulation Study. *J. Chem. Phys.* **2000**, *113*, 2814–2822.
- (23) Wensink, E. J. W.; Hoffmann, A. C.; Maaren, P. J. v.; Spoel, D. v. e. Dynamic Properties of Water/Alcohol Mixtures Studied by Computer Simulation. *J. Chem. Phys.* **2003**, *119*, 7308–7317.
- (24) Noskov, S. Y.; Lamoureux, G.; Roux, B. Molecular Dynamics Study of Hydration in Ethanol–Water Mixtures Using a Polarizable Force Field. *J. Phys. Chem. B* **2004**, *109*, 6705–6713.
- (25) Wang, S.; Cann, N. M. Polarizable and Flexible Model for Ethanol. *J. Chem. Phys.* **2007**, *126*, 214502–214524.
- (26) Gonzalez, M. A.; Enciso, E.; Bermejo, F. J.; Bee, M. Ethanol Force Fields: A Molecular Dynamics Study of Polarization Effects on Different Phases. *J. Chem. Phys.* **1999**, *110*, 8045–8059.
- (27) Jorgensen, W. L. Optimized Intermolecular Potential Functions for Liquid Alcohols. *J. Phys. Chem.* **1986**, *90*, 1276–1284.
- (28) Smith, B. D.; Srivastava, R. *Thermodynamic Data for Pure Compounds*; Elsevier: Amsterdam, The Netherlands, 1986.
- (29) Meckl, S.; Zeidler, M. D. Self-Diffusion Measurements of Ethanol and Propanol. *Mol. Phys.* **1988**, *63*, 85–95.
- (30) Marti, J.; Guardia, E.; Padro, J. A. Dielectric Properties and Infrared Spectra of Liquid Water: Influence of the Dynamic Cross Correlations. *J. Chem. Phys.* **1994**, *101*, 10883–10891.
- (31) Svishchev, I. M.; Kusalik, P. G.; Wang, J.; Boyd, R. J. Polarizable Point-Charge Model for Water: Results under Normal and Extreme Conditions. *J. Chem. Phys.* **1996**, *105*, 4742–4750.
- (32) Lamoureux, G.; Roux, B. Modeling Induced Polarization with Classical Drude Oscillators: Theory and Molecular Dynamics Simulation Algorithm. *J. Chem. Phys.* **2003**, *119*, 3025–3039.
- (33) Rullmann, J. A. C.; Duijnen, P. T. v. A Polarizable Water Model for Calculation of Hydration Energies. *Mol. Phys.* **1988**, *63*, 451–475.
- (34) Rick, S. W.; Stuart, S. J.; Berne, B. J. Dynamical Fluctuating Charge Force Fields: Application to Liquid Water. *J. Chem. Phys.* **1994**, *101*, 6141–6156.
- (35) Andoh, Y.; Kurahashi, K.; Sakuma, H.; Yasuoka, K.; Kurihara, K. Anisotropic Molecular Clustering in Liquid Ethanol Induced by a Charged Fully Hydroxylated Silicon Dioxide (SiO₂) Surface. *Chem. Phys. Lett.* **2007**, *448*, 253–257.
- (36) Cooke, D. J.; Gray, R. J.; Sand, K. K.; Stipp, S. L. S.; Elliott, J. A. Interaction of Ethanol and Water with the (1014) Surface of Calcite. *Langmuir* **2010**, *26*, 14520–14529.
- (37) Rossetto, H. L.; Bowen, J.; Kendall, K. Adhesion of Alumina Surfaces through Confined Water Layers Containing Various Molecules. *Langmuir* **2012**, *28*, 4648–4653.
- (38) Sung, J.; Waychunas, G. A.; Shen, Y. R. Surface-Induced Anisotropic Orientations of Interfacial Ethanol Molecules at Air/

Sapphire (1102) and Ethanol/Sapphire(1102) Interfaces. *J. Phys. Chem. Lett.* **2011**, *2*, 1831–1835.

(39) Tobbens, D. M.; Stusser, N.; Knorr, K.; Mayer, H. M.; Lampert, G. E9: The New High-Resolution Neutron Powder Diffractometer at the Berlin Neutron Scattering Center. *Mater. Sci. Forum* **2001**, 378–3, 288–293.

(40) Coustet, V.; Jupille, J. High-Resolution Electron-Energy-Loss Spectroscopy of Isolated Hydroxyl-Groups on α -Al₂O₃ (0001). *Surf. Sci.* **1994**, *309*, 1161–1165.

(41) Sung, J.; Zhang, L.; Tian, C.; Waychunas, G. A.; Shen, Y. R. Surface Structure of Protonated R-Sapphire (1102) Studied by Sum-frequency Vibrational Spectroscopy. *J. Am. Chem. Soc.* **2011**, *133*, 3846–3853.

(42) Trainor, T. P.; Eng, P. J.; Brown, G. E., Jr.; Robinson, I. K.; Santis, M. D. Crystal Truncation Rod Diffraction Study of the α -Al₂O₃ (1 $\bar{1}$ 02) Surface. *Surf. Sci.* **2002**, *496*, 238–250.

(43) Cygan, R. T.; Liang, J. J.; Kalinichev, A. G. Molecular Models of Hydroxide, Oxyhydroxide, and Clay Phases and the Development of a General Force Field. *J. Phys. Chem. B* **2004**, *108*, 1255–1266.

(44) Schweighofer, K. J.; Essmann, U.; Berkowitz, M. Simulation of Sodium Dodecyl Sulfate at the Water–Vapor and Water–Carbon Tetrachloride Interfaces at Low Surface Coverage. *J. Phys. Chem. B* **1997**, *101*, 3793–3799.

(45) Hess, B.; Bekker, H.; Berendsen, H. J. C.; Fraaije, J. G. E. M. LINCS: A Linear Constraint Solver for Molecular Simulations. *J. Comput. Chem.* **1997**, *18*, 1463–1472.

(46) Allen, M. P.; Tildesley, D. J. *Computer Simulation of Liquids*; Oxford University Press, Oxford, 2004.

(47) Essmann, U.; Perera, L.; Berkowitz, M. L.; Darden, T.; Lee, H.; Pedersen, L. G. A Smooth Particle Mesh Ewald Method. *J. Chem. Phys.* **1995**, *103*, 8577–8593.

(48) Hoover, W. G. Canonical Dynamics—Equilibrium Phase-Space Distributions. *Phys. Rev. A* **1985**, *31*, 1695–1697.

(49) Nose, S. A Molecular-Dynamics Method for Simulations in the Canonical Ensemble. *Mol. Phys.* **1984**, *52*, 255–268.

(50) Hess, B.; Kutzner, C.; Van der Spoel, D.; Lindahl, E. GROMACS 4: Algorithms for Highly Efficient, Load-Balanced, and Scalable Molecular Simulation. *J. Chem. Theory. Comput.* **2008**, *4*, 435–447.

(51) Van der Spoel, D.; Lindahl, E.; Hess, B.; Groenhof, G.; Mark, A. E.; Berendsen, H. J. C. GROMACS: Fast, Flexible, and Free. *J. Comput. Chem.* **2005**, *26*, 1701–1718.

(52) Mezei, M.; Beveridge, D. L. Theoretical-Studies of Hydrogen-Bonding in Liquid Water and Dilute Aqueous-Solutions. *J. Chem. Phys.* **1981**, *74*, 622–632.

(53) Kumar, R.; Schmidt, J. R.; Skinner, J. L. Hydrogen Bonding Definitions and Dynamics in Liquid Water. *J. Chem. Phys.* **2007**, *126*, 204107–204118.

(54) Auer, B. M.; Skinner, J. L. Water: Hydrogen Bonding and Vibrational Spectroscopy, in the Bulk Liquid and at the Liquid/Vapor Interface. *Chem. Phys. Lett.* **2009**, *470*, 13–20.

(55) Lange, N. A.; Dean, J. A. *Lange's Handbook of Chemistry*, 10th ed; McGraw-Hill, New York, 1967.

(56) Marrink, S. J.; Berendsen, H. J. C. Simulation of Water Transport through a Lipid- Membrane. *J. Phys. Chem.* **1994**, *98*, 4155–4168.

(57) Argyris, D.; Cole, D. R.; Striolo, A. Dynamic Behavior of Interfacial Water at the Silica Surface. *J. Phys. Chem. C* **2009**, *113*, 19591–19600.

(58) Catalano, J. G.; Park, C.; Zhang, Z.; Fenter, P. Termination and Water Adsorption at the Alpha-Al₂O₃ (012)—Aqueous Solution Interface. *Langmuir* **2006**, *22*, 4668–4673.

(59) Catalano, J. G. Relaxations and Interfacial Water Ordering at the Corundum (110) Surface. *J. Phys. Chem. C* **2010**, *114*, 6624–6630.

(60) Catalano, J. G.; Fenter, P.; Park, C. Interfacial Water Structure on the (012) Surface of Hematite: Ordering and Reactivity in Comparison with Corundum. *Geochim. Cosmochim. Acta* **2007**, *71*, 5313–5324.